Channel-Aware Rate Adaptation for Backscatter Networks

Wei Gong, *Member, IEEE*, Haoxiang Liu, Jiangchuan Liu, *Fellow, IEEE*, Xiaoyi Fan, *Student Member, IEEE*, Kebin Liu, *Member, IEEE*, Qiang Ma, *Member, IEEE*, and Xiaoyu Ji, *Member, IEEE,*

***Abstract*— Backscatter communication networks receive much attention recently due to the small size and low power of backscatter nodes. As backscatter communication is often influenced by the dynamic wireless channel quality, rate adaptation becomes necessary. Most existing approaches share a common drawback: they fail to take both spatial and frequency diversity into consideration at the same time. Consequently, the transmission rate may be improperly selected, resulting in low network throughput. In this paper, we propose a channel-aware rate adaptation framework (CARA) for backscatter networks. CARA incorporates three essential modules, a lightweight channel probing scheme that differentiates collisions from packet losses, a burstiness-aware channel selection mechanism benefiting as many backscatter nodes as possible, a rate selection method choosing the optimal rate, and a mobility detection that discovers location changes. We implement CARA on commercial readers, and the experiment results show that CARA achieves up to 4× goodput gain compared with the state-of-the-art rate adaptation scheme.**

***Index Terms*— Backscatter communication, frequency selection, RFID, tags.**

I. Introduction

BACKSCATTER communication networks, e.g., RFID systems, are widely deployed to build sensing and computational platforms [1]–[3]. Due to the small size and low power consumption of backscatter nodes, they can be implanted in objects to perform a variety of tasks. Typically, sensor-integrated backscatter nodes enable pervasive sensing [4], [5]. For example, we can embed a grid of nodes into walls to monitor the structural deformation [6]. Also, we can implant nodes into animal's brain to sense the neural condition [7]. Although backscatter nodes virtually perform the same tasks as traditional sensing devices, e.g., motes, they have significant advantages due to power efficiency.

Rate adaptation in backscatter communication networks is essential for two reasons. First, backscatter nodes transmit sensing data with energy harvested from the reader's RF signal. This low power feature makes the communication quite vulnerable to the dynamic channel quality. Second, backscatter communication networks are usually deployed in complex scenarios, like indoor environments. As a result, the channel quality is affected by multiple factors, such as blocking, multipath fading, external interference etc. Therefore, to ensure high network throughput, it is important to adapt the data rate according to dynamic channel qualities.

Rate adaptation is a non-trivial problem due to the channel diversity, namely *spatial diversity* and *frequency diversity*. On one hand, channel qualities are different due to locations. Nodes are scattered in different locations, thus they experience diverse channel qualities due to channel fading and multipath effect [8]. This phenomenon is denoted as *spatial diversity*. On the other hand, channel qualities are different due to different center-frequencies, even for the same node. Such differences are mainly caused by frequency selective fading [8], which means the frequency response is not flat. This kind of diversity is called *frequency diversity*.

Most existing rate adaptation approaches in backscatter communication networks, however, lack the consideration of either spatial diversity or frequency diversity. As a result, the transmission rate may be improperly selected, leading to network throughput degradation. In [9], a link layer named BLINK is designed for backscatter communication networks. BLINK assumes that all backscatter nodes experience the same channel quality. Another work, Buzz [10], takes advantage of rateless code to address the rate adaptation problem. It models the network as a single tap channel, ignoring the impact of frequency diversity. According to our experimental studies in Section II-B, both assumptions in BLINK and Buzz could be invalid in common scenarios.

In this paper, we propose a Channel-Aware Rate Adaptation framework (CARA) for backscatter communication networks, which effectively exploits both spatial and frequency diversity to maximize the network throughput. In order to select appropriate transmission rates, several challenges must be addressed, such as channel quality estimation, link burstiness, and rate selection. In CARA, we design a lightweight channel probing scheme that obtains fine-grained channel metrics, including RSSI and packet loss rate, to enable accurate

Manuscript received October 6, 2016; revised October 28, 2017; accepted January 11, 2018; approved by IEEE/ACM TRANSACTIONS ON NETWORKING Editor K. Psounis. Date of publication February 27, 2018; date of current version April 16, 2018. This work was supported in part by the Canada Technology Demonstration Program Grant, in part by the Canada NSERC Discovery Grant, in part by the NSERC E.W.R. Steacie Memorial Fellowship, and in part by NSFC under Grant 61472268. *(Corresponding author: Jiangchuan Liu.)*

W. Gong, J. Liu, and X. Fan are with the School of Computing Science, Simon Fraser University, Burnaby, BC V5A 1S6, Canada (e-mail: gongweig@sfu.ca; jcliu@sfu.ca; xiaoyif@sfu.ca).

H. Liu is with the Department of Computer Science and Engineering, The Hong Kong University of Science and Technology, Hong Kong (e-mail: haoxiang@greenorbs.com).

K. Liu and Q. Ma are with the School of Software, Tsinghua National Laboratory for Information Science and Technology, Tsinghua University, Beijin 100084, China (e-mail: kebin@greenorbs.com; maq@greenorbs.com).

X. Ji is with the College of Electrical Engineering, Zhejiang University, Hangzhou 310027, China (e-mail: jixiaoyu.hk@gmail.com).

Digital Object Identifier 10.1109/TNET.2018.2802323

Channel Number	Center Frequency (MHz)
3	920.625
4	920.875
...	...
17	924.125
18	924.375

Fig. 1. UHF RFID channels for China.

channel estimation. Also, a new measurement model is built to assess the contributions to packet loss due to path loss and collisions, providing more accurate channel estimates. Then, we introduce a novel burstiness-aware channel selection algorithm to effectively select a subset of channels that cover all the backscatter nodes. The insight of our channel selection algorithm is to employ "consistently good" links as many as possible and to discard "consistently bad" links. Last, we train a K-nearest-neighbors classifier to select the optimal data rate with respect to the node with the best channel condition. The whole framework is prototyped on an Impinj Speedway reader. The evaluation results show that our mechanism achieves up to $4\times$ goodput gain compared with state-of-the-art scheme BLINK.

II. Background and Motivation

A. Backscatter Communication

Following the Open Systems Interconnection (OSI) model, we describe the backscatter communication from the physical layer and the data link layer. Here we focus on the C1G2 standard, which is one of the most widely used RFID protocols in the world [11].

Physical Layer: In backscatter networks, the physical layer of the forward link (reader to backscatter nodes) and backward link (backscatter nodes to the reader) use different data encoding schemes. The forward links use pulse-interval encoding (PIE). The backward links use more complex encoding schemes such as FM0 and Miller. The rate adaptation, including this work, primarily focuses how to choose the best rate that is fit for the current channel condition and thus to maximize the overall throughput. Same as previous work [9], this paper mainly deals with the backward link, because the backscatter signal is more vulnerable to the channel dynamics. Another important feature of backscatter systems is channel hopping. Although the tag can respond in all the channels, it would experience different channel qualities. The tag itself cannot choose channels because it does not generate its own radios but only backscatters the incoming waves from the reader. The reader, however, has the ability to hop across a bunch of channels. For example, according to regulations in China, there are 16 available channels as in Figure 1. In North America, FCC specifies 50 channels for UHF RFID.

Data Link Layer: Media access control (MAC) is the most important part of the data link layer. The C1G2 standard specifies a slotted ALOHA MAC. It works as follows. First, the reader initiates the communication with a *Query* message,

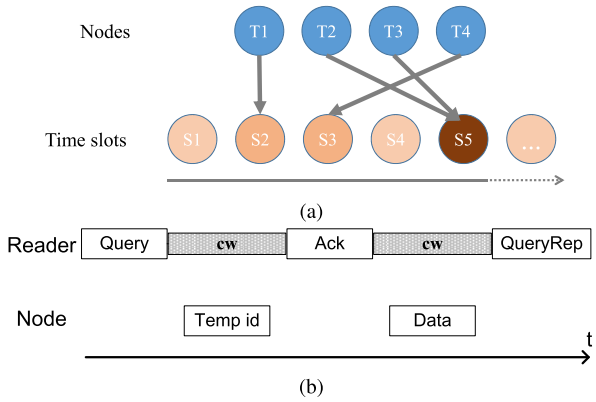

Fig. 2. Data link model of backscatter communication. (a) Medium access control in backscatter systems. (b) An example of the data link without collisions.

which includes a parameter Q to assign 2^Q time slots. Each node, upon receiving this message, randomly chooses a time slot to reply a 16-bit temporary id. This may result in three different statues for the slot. As shown in Figure 2a, S1 and S4 are empty slots that have no reply. S2 and S3 are singleton slots that have only one node's reply, which means T1 and T4 have been granted the right to use the medium. S5 is a collision slot that has more than one node's reply, which means neither T2 nor T3 succeeded in competing. For the node that is in the singleton slot, the reader can further request the node's data, which is illustrated in Figure 2b.

B. Empirical Study and Motivation

We first empirically measure the channel diversity in backscatter communication networks from two aspects, namely spatial and frequency diversity. We conduct experiments using an Impinj Speedway reader and a bunch of Impinj Inlay passive tags. Please note that as similar observations are made in a series of experiments, for brevity we highlight a typical one here.

In this setting, we randomly place 9 tags in front of the reader, with distances of 3-5 meters. The tags have different distances and angles towards the reader antenna and thus experience diverse channel qualities. We also place some objects around the tags to create multipath effects.

Observations: We let the reader read the tags for 15 seconds and record the reading rate for each tag across the 16 available channels. The reading rate can be explained as the ratio of the total number of EPCs (Electronic Product Code, the unique identifier for each tag) captured by the reader to the reading time. The experiment results are shown in Figure 3. We have the following observations. First, for each tag, the reading rate varies across the 16 channels, reflecting frequency diversity. Take tag 1 as an example. Channel 1-6 can be regarded as good channels, while channel 9-14 are poor in comparison. Typically, the reading rate of the best channel (channel 2) is 9.5 times faster than the worst one (channel 14). The frequency diversity is mainly due to frequency selective fading.

Second, different tags have diverse responses to the channels, showing spatial diversity. For example, given channel 15,

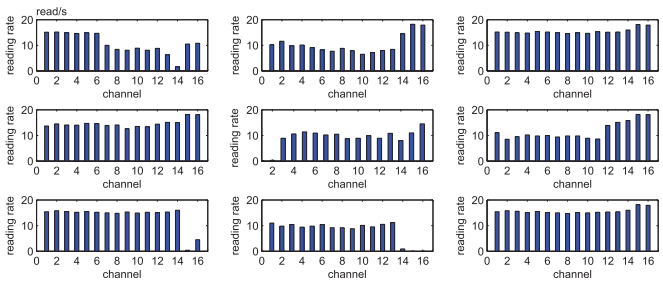

Fig. 3. The spatial and frequency diversity of backscatter link quality. *For each specific backscatter node, the channel quality varies among different channels. For a specific channel, different backscatter nodes have diverse channel qualities.*

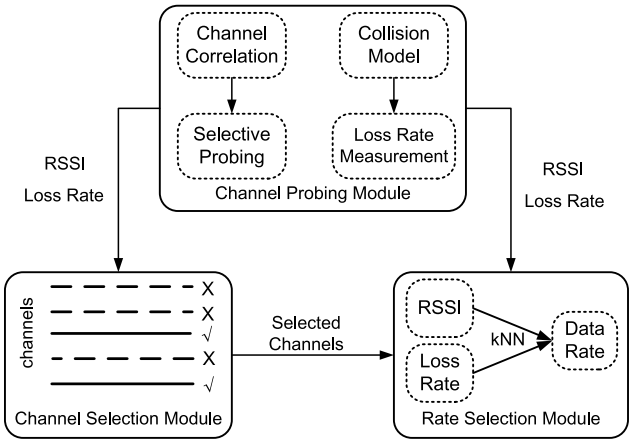

Fig. 4. CARA framework overview.

the reading rates of tag 7 and tag 8 are very low, whereas they are high for the other tags. This is because the tags have different distances and orientations to the reader antenna. In addition, multipath fading is also position specific.

These two observations imply that the rate adaptation scheme can take advantage of such channel diversity that is due to different frequencies and spatial locations, which is the major motivation of this work. In contrast, the previous rate adaptation mechanisms in backscatter networks do not have a complete view of such channel diversity [9] [10]. Note that the phenomena of both frequency and spatial diversity are well-known for wireless communication [8]. The purpose of this work is to examine how these phenomena behave in backscatter systems and then find a way to deal with them for rate adaptation.

III. Channel-Aware Rate Adaptation

We propose a channel-aware rate adaptation framework, CARA, in backscatter communication networks. Our design goal is to maximize throughput using rate control for static scenarios (both readers and nodes). CARA consists of three components: channel probing, channel selection, and rate selection.

A. Design Overview

Figure 4 plots the CARA framework. The basis of CARA lies in channel probing since accurate channel estimation results in appropriate channel and rate selection. Our channel probing scheme takes advantage of channel correlation to reduce probing overhead. Additionally, we propose a node collision model to calculate the packet loss rate due to path loss. The probing results, including RSSI and packet loss rate, are imported to channel selection and rate selection module. The channel selection module selects a subset of good channels. In the rate selection module, the RSSI and packet loss rate are mapped to an appropriate data rate via a K-nearest-neighbor classifier.

B. Channel Metrics

To describe the channel quality, frequently used metrics include signal-to-noise ratio (SNR), received signal strength indicator (RSSI), bit error rate (BER), and packet loss rate. Among these four metrics, SNR and BER need special hardware support and therefore cannot be easily obtained in backscatter communication networks. RSSI is provided by commercial readers. However, RSSI alone cannot accurately reflect channel quality because of multipath effects. Generally, the received signal is the sum of signals traveling via different paths. Hence, it is possible that the received signal has a high RSSI but still cannot be decoded, indicating poor channel quality. Therefore, we introduce packet loss rate as a complementary metric to RSSI. Besides collisions on the MAC layer, the loss rate in backscatters system has two main contributions on the physical layer, path loss and multipath fading (including multipath self-interference) [9]. Other contributions include interference and environmental changes.

C. Channel Probing Scheme

In this section, we introduce a lightweight channel probing scheme to measure the RSSI and packet loss rate.

1) Probing Overhead: The main objective of channel probing is to obtain accurate channel metrics. Since spatial and frequency diversity exists, it is desirable to obtain the metrics per channel and per node. An intuitive approach is to inject a lot of probe packets into each available channel and calculate the packet loss rate and average RSSI for each node. However, this would incur a significant overhead that comes from two aspects. First, the probing overhead grows with the number of channels. Second, the more accurate results we want, the more probe packets are required. Insufficient probes will result in inaccurate metrics. BLINK proposes to obtain the channel metrics using only one probe. We argue that it is insufficient and more probes are needed. For example, suppose there is one backscatter node in the network and the reader sends merely one probe, there are totally 2 situations: either 0 or 1 reply from the node will be received by the reader. The consequent loss rate is either 100% or 0%, which cannot reflect the channel quality in fine granularity. More importantly, the situation gets worse as the number of nodes increases. In backscatter networks, nodes are unable to sense each other, so that collision is inevitable. It is apparent that the one-probe approach does not fit for multiple nodes scenarios, since packet loss may be caused by the collision instead of poor channel quality.

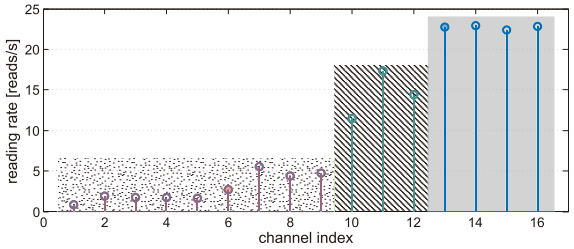

Fig. 5. A typical example of channel correlation.

TABLE I
DISTRIBUTION OF CCN

CCN value	Percentage
1	4.7%
2	11.9%
3	7.1%
4	14.3%
5	9.5%
≥ 6	52.5%

2) Selective Probing: To reduce the probing overhead, we discover that it is not necessary to probe all the channels since the adjacent channels often exhibit similar qualities. We propose a lightweight probing strategy called selective probing.

We define that two channels are correlated if the difference of reading rates is within a predefined threshold t. We propose an indicator that describes the channel correlation, called Correlated Channel Number (CCN). More precisely, CCN is denoted as the number of consecutive correlated channels. To verify channel correlation, we place a passive tag in various positions and use the reader to read the tag for 10 seconds in each of the 16 channels. The threshold t is set to 5 reads/s. In Figure 5 the result of a typical experiment is presented. We observe that the adjacent channels do exhibit similarity despite the diversity across all channels. Particularly, the 16 channels fall into three groups. The first group contains channel 1-9, which exhibit poor channel quality. The second group contains intermediate channels including channel 10-12. The remaining channels form the third group. Also, there are two change points of channel quality, which are between channel 9-10 and 12-13. The minimum CCN of this case is 3.

Taking all the experiments together, the distribution of measured CCN is shown in Table I. By exploiting channel correlation, we propose an online selective probing algorithm to reduce the probing overhead. The basic idea is that we probe the channels at regular interval d. d is chosen so that it is below most CCN values. When we probe a new channel and the difference between its quality and the last probe is beyond the threshold t, we can infer that this interval contains a change point cp. cp can be located by probing like binary search.[1] In this way, we divide the channels into groups separated by change points. The channel qualities in the same group are derived using just one probe. Thus, the probing overhead is alleviated.

[1]The probing interval is properly chosen such that there exists only one change point in the interval

3) Packet Loss Rate Calibration: Packet loss rate is adopted as a metric to estimate the channel quality. However, it is a biased estimator if used directly from channel probing. This is because packet loss is not only caused by poor channel quality, but also backscatter node collision. In particular, the measured packet loss rate p can be derived by combining the path loss rate p_p (for channel quality) and collision loss rate p_c (for collision). The transmission rate should be adjusted to channel quality, without the impact of collisions. Therefore, to exactly reflect path loss rate p_p, the impact of node collision should be accounted for as shown in Equation 1.

$$p_p = 1 - \frac{1-p}{1-p_c} \tag{1}$$

In Equation 1, p can be measured directly by probing and p_c is unknown. To estimate p_c, we build an approximate model for node collision. As specified by the EPC Class-1 Gen-2 standard [11], each backscatter node randomly selects a slot from the frame to respond. We call the slot that contains one response a *singleton* slot. Then the expected number of singleton slots in the frame is:

$$n_s = m(1 - \frac{1}{2^Q})^{(m-1)} \tag{2}$$

where 2^Q is the frame size and m is the number of backscatter nodes. Then, the expected number of responses from each node is given by $(1 - \frac{1}{2^Q})^{(m-1)}$, which is p_c. Obviously, we need the values of m and Q to calculate p_c. In practice, m can often be known as a priori. For example, we always know the number of deployed sensor nodes from which to collect sensing data. Obtaining Q, however, is difficult since the reader does not expose the parameter to users. We propose an empirical value of Q as follows:

$$Q = \underset{Q}{\operatorname{argmin}}\ 2^Q > m \tag{3}$$

The intuition is that the reader would choose the shortest frame that contains as many singleton slots as possible. The validation of this proposed model is left in the evaluation section. It is worth noting that the packet loss rate refers to the calibrated rate (path loss rate) in the rest of this paper unless otherwise indicated.

4) Probing Time: There is yet another question remaining: how long is enough to probe one channel to achieve accurate loss rate measurement (we focus on loss rate because RSSI is relatively stable)? Intuitively, the longer the probing time, the more precise results we obtain. However, it is a tradeoff since long probing time incurs heavy overhead and therefore low throughput. To address this problem, we experimentally show how to properly choose probing time in the evaluation.

D. Burstiness-Aware Channel Selection

For simplicity, we first describe our channel selection in an ideal case (without considering link burstiness) and then extend it to account for bursty links. Due to frequency diversity, some frequencies may not be suitable for transmission

thus should be avoided. Therefore, we design a channel selection algorithm to choose a set of good channels that cover all backscatter nodes. Nodes and channels are mutually related. Namely, each node has several good channels and each channel shows good effects on some nodes. To present this relation, we construct a $m \times k$ matrix $\mathbf{C}$ from the channel probing results, where m and k are the numbers of nodes and available channels respectively. In $\mathbf{C}$, we have

$$\mathbf{C}_{\mu,\nu} = \begin{cases} 1 & \text{if } \nu \in G_\mu \\ 0 & \text{otherwise} \end{cases}$$

where G_μ is the set of good channels for node μ. More precisely, $\mathbf{C}_{\mu,\nu}$ is set to 1 if channel ν is one of the good channels for node μ [2]. Our objective now is to select the minimum number of good channels that cover all the backscatter nodes. Therefore, formally we have the following optimization problem:

$$Minimize \sum_{i=1}^{k} \mathbf{x}_i \tag{4}$$

Subject to the constraints that

$$\begin{aligned} \mathbf{C} \cdot \mathbf{x} &\geq \mathbf{I} \\ \mathbf{x}_i &\in \{0,1\} \quad 1 \leq i \leq k \end{aligned} \tag{5}$$

where $\mathbf{x}$ is a vector that determines which channels should be selected and $\mathbf{I}$ is a unit vector. This optimization problem is analogous to the typical *set cover problem*, which in NP-complete [12]. Since it is an NP-complete problem, we design an approximation greedy algorithm to solve it. The algorithm works as follows. For each column ν in $\mathbf{C}$, we construct a set S_ν, and $S_\nu = \{\mu \mid 1 \leq \mu \leq m, \mathbf{C}_{\mu,\nu} \neq 0\}$. As a result, we obtain k sets, namely $S_\nu, 1 \leq \nu \leq k$. The union $\bigcup S_\nu$ is the node set $U = \{1, 2, \ldots, m\}$. The algorithm iteratively chooses the largest set among the unselected sets until all elements in U are covered. After each iteration, the covered elements in U are removed from each unselected set. This greedy algorithm is inspired by [12], where the analysis shows its approximation ratio is $\ln(m)$.

So far, we have not considered link burstiness yet, which is an important feature of wireless links [13]. We use a well-known metric, β [13], to quantify link burstiness. In particular, it is defined as follows, $\beta = \frac{\mathbf{KW}(I) - \mathbf{KW}(E)}{\mathbf{KW}(I)}$, where $\mathbf{KW}()$ denotes the Kantorovich-Wasserstein distance from the ideal bursty link [14], E is the Conditional Packet Delivery Function (CPDF) of the empirical link in tests, and I is the CPDF of an independent link with the same packet reception ratio. An example of beta calculation is shown in Figure 6. Note that an ideal bursty link is a link that has a long burst of either successes or failures, i.e., all successes or all failures.

Based on the above beta definition, we set up a threshold for burstiness, β_{hi}, and another two thresholds for packet reception ratio, ξ_{hi} and ξ_{lo}. Accordingly, we can classify links into three groups, the high-quality link that is with a burstiness more than β_{hi} and a packet reception ratio more than ξ_{hi},

[2]In this paper, we specifically use μ for node indexing and ν for channel indexing.

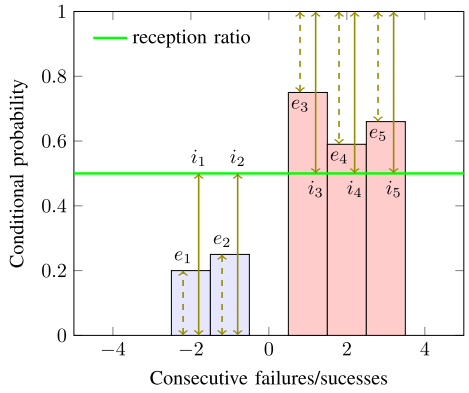

Fig. 6. β calculation for an example link. The overall reception ratio is the green line. e_i $(i = 1, \ldots, 5)$ is the distance between the i-th CPDF element of the example link and the i-th CPDF element of the ideal bursty link. Likewise, i_j $(j = 1, \ldots, 5)$ is the distance between the j-th CPDF element of the corresponding independent link and the j-th CPDF element of the ideal bursty link. Hence, $\beta = \frac{\text{mean}(i_1,\ldots,i_5) - \text{mean}(e_1,\ldots,e_5)}{\text{mean}(i_1,\ldots,i_5)} = 0.42$.

the low-quality link that is with a burstiness more than β_{hi} and a packet reception ratio less than ξ_{low}, the intermediate link that is not included in the former two groups. The intuition behind this classification is straightforward. The high-quality link should be consistently good (a high β and a high ξ) while the low-quality link is consistently bad (a high β and a low ξ). The examples of measured links are shown in Figure 7.

Based on the above classification, modifying Algorithm 1 to account for burstiness is easy. After we obtain the three groups of links, we run Algorithm 1 only based on the group of high quality links first. If it covers all the nodes then returns, otherwise, it continues to pick up candidates from the group of intermediate links. Note that in our scheme low quality links are avoided.

In some cases where most links are of low quality, we may resort to a conservative scheme. Specifically, we can keep at the lowest rate and randomly hop across all channels because the current channel condition is so harsh (all the links are poor). Such a scheme is fit for applications where the reliable communication is the top priority, such as emergency rescue or military.

Another thing worth noting is that our channel selection scheme may seem similar to Adaptive Frequency Hopping (AFH) for Bluetooth [15]–[17] because both schemes use RSSI and packet loss rate to assess channels and then to avoid bad channels. There are, however, several differences. First, the packet loss-rate measurement in Bluetooth does not need to combat collisions while we need to calibrate it with collision estimates. Second, AFH is for point-to-point communication whereas our scheme is for one(reader)-to-many(tags).

E. Rate Selection

Rate selection module exploits the channel metric (RSSI and packet loss rate) to determine a data rate. As specified in the EPC Class-1 Gen-2 standard, there are various bit-rates to select from for the backward link, which is jointly determined by the baudrate and encoding scheme as presented in Table II. The bit-rate ranges from 40kbps to 640kbps.

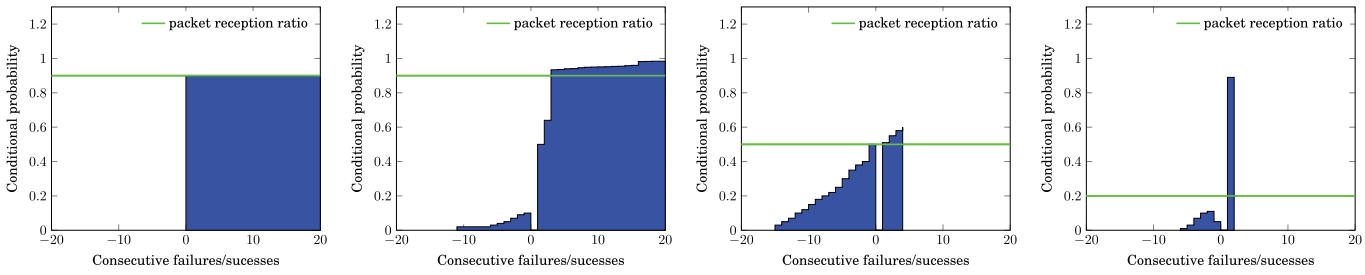

Fig. 7. Examples of measured backscatter links. (a) an ideal bursty link with $\beta = 1, \xi = 0.9$; (b) a high quality link with $\beta = 0.82, \xi = 0.9$; (c) an intermediate link with $\beta = 0.47, \xi = 0.5$; (d) a low quality link with $\beta = 0.76, \xi = 0.2$;

TABLE II
BACKWARD LINK DATA RATES IN EPC GEN-2 STANDARD

Encoding scheme	Baudrate
FM0 baseband	bit rate
Miller2	bit rate/2
Miller4	bit rate/4
Miller8	bit rate/8

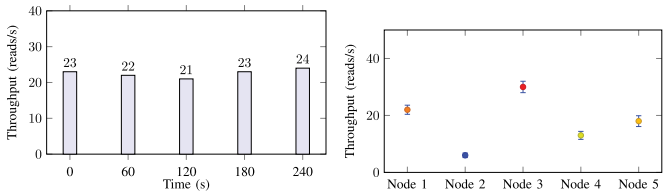

Fig. 8. Channel variability in terms of throughput. (a) Throughput variation over time. (b) Throughput variations for different nodes.

1) Channel Metric Classifier: Given RSSI and packet loss rate, we seek to map these channel metrics to optimal data rates. The well-known K-nearest neighbors (kNN) classifier is utilized to perform such mapping. Briefly, this is a two-phase process including a training phase and a classification phase. To train the classifier, we collect channel features in various environments and label them with the corresponding optimal data rates. In classification phase, we input the current channel metrics to the kNN classifier which outputs the optimal data rate. In kNN, we define the distance between two feature vectors $(RSSI_1, lr_1)$ and $(RSSI_2, lr_2)$ in kNN classifier as $\sqrt{(RSSI_1 - RSSI_2)^2 + \alpha(lr_1 - lr_2)^2}$ where $RSSI$ and lr denote RSSI and loss rate, respectively. The weights α is introduced since loss rate is a dominant factor. In the implementation, we empirically choose the values of α.

2) Channel-Aware Rate Selection: Using the classifier, we obtain the optimal data rate for each backscatter node on each selected channel. Let k' be the number of selected channels, and $(RSSI, lr)_{i,j}$ be the channel metrics with respect to the i^{th} node and j^{th} selected channel. The mapping from channel metrics to data rates is shown in the matrix representation below.

$$\begin{bmatrix} (RSSI,lr)_{1,1} & (RSSI,lr)_{1,2} & \cdots & (RSSI,lr)_{1,k'} \\ (RSSI,lr)_{2,1} & (RSSI,lr)_{2,2} & \cdots & (RSSI,lr)_{2,k'} \\ \vdots & \vdots & \ddots & \vdots \\ (RSSI,lr)_{m,1} & (RSSI,lr)_{m,2} & \cdots & (RSSI,lr)_{m,k'} \end{bmatrix} \Rightarrow \begin{bmatrix} r_{1,1} & r_{1,2} & \cdots & r_{1,k'} \\ r_{2,1} & r_{2,2} & \cdots & r_{2,k'} \\ \vdots & \vdots & \ddots & \vdots \\ r_{m,1} & r_{m,2} & \cdots & r_{m,k'} \end{bmatrix} = \mathbf{R}$$

where $\mathbf{R}$ is the optimal data rate matrix.

Although we have $\mathbf{R}$, it is not allowed to assign a unique data rate for each node. According to the EPC Class-1 Gen-2 standard, the reader specifies a single data rate for all nodes every time. Despite this constraint, we are still flexible to uniquely choose a data rate for each selected channel. In CARA, we greedily choose the highest data rate among all nodes' optimal data rates for each channel, i.e., $max(\mathbf{R}_{ij})$ for each j. But a prerequisite for this choice is that the candidate rate should be the best rate for at least one-third of nodes, otherwise we choose the rate with the highest number of nodes. The intuition is that in each selected channel, there exist several nodes that have good transmission rates. We should satisfy their optimal rates in the first place to achieve high throughput. Such a heuristic helps to improve the overall throughput of the network.

F. Mobility Detection

Now, we come to the final question that is when to probe. First, we examine how channel varies over time in terms of throughput. Note that the channel variation measured here focuses on the throughput, but not the fine-grained channel coherence for demodulation [8], because our rate adaptation is for maximizing throughput. We measure a static node's throughput at different times, namely, 0s, 60s, 120s, 180s, and 240s and the results are shown in Figure 8a. We observe that the node's throughput is quite stable on the order of minutes. We further test more nodes at different locations(each for 4 minutes) and present 5 representatives in Figure 8b. We find that channel variation in terms of throughput is really concentrated. Thus, we can regularly probe the channel every few minutes.

In some scenarios, however, the node may be moved or replaced, which may cause large variation of channels. Therefore, a mobility detection scheme becomes necessary as an additional trigger for re-probing if the location of a node has changed. For example, in the library, books

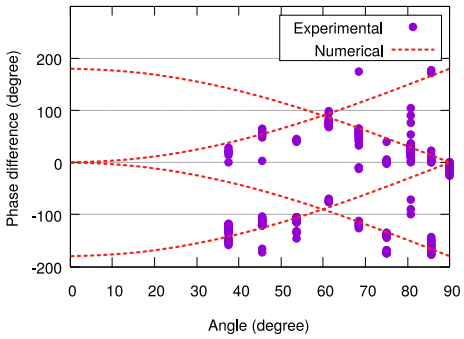

Fig. 9. Measured phase differences on two receiving reader antennas for a single static tag. Results are obtained at the same distance but different angles. While previous schemes [18] have the same assumption that phase differences should be stable if the tag is static (at a fixed angle), it is challenged in typical indoor office environments. Large deviations between experimental measurements (purple dots) and theoretical values (dotted red lines) exist in almost all cases, which means the phase differences is not always a good indicator of the angle/position change.

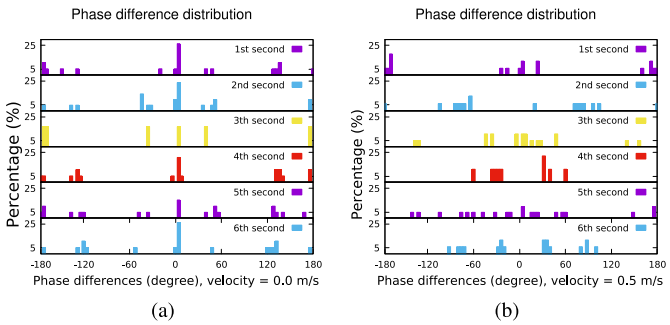

Fig. 10. Histograms of different time intervals for a static tag (a) and a mobile tag (b). For the static tag, the histograms are similar across different time intervals, while those of the mobile tag are quite different.

(with RFID tags) easily get displaced by casual readers. Note that similar to the same module in BLINK [9], our mobility detection is not to detect the velocity or other mobility metrics but only the location change. While several advanced backscatter localization methods provide centimeter or even millimeter accuracy [18], [19], they are not lightweight enough to fit our rate adaptation framework. The state-of-the-art solution, BLINK [9], provides a lightweight method based on RSSI values and loss rate. Yet, it suffers increasing false alarms from environmental mobility, which is not negligible.

In contrast, we propose a new mobility detection scheme that is robust to environmental mobility and achieves almost zero overhead. The core of our mobility detection is using phase values of backscatter signals, which are not affected by environmental factors and easy to obtain in most off-the-shelf readers [20], [21]. However, it would be erroneous if we directly relate phase values or phase differences to locations of objects. As shown in Figure 9, the phase differences of the static tag are not stable in a typical indoor environment.

However, we observe that although a single phase difference value may not be a good base for inferring locations, the histogram of phase differences over a short interval is quite stable if the tag is static, and when the tag is mobile, the corresponding histogram changes significantly. The results of this observation are shown in Figure 10. Such an observation motivates us to use the similarity of histograms to detect mobility. Therefore, we use the well-known Bhattacharyya distance [22] to measure the similarity between two histograms. Given two consecutive measured histograms, $\Omega^i = \{\omega_1^i, \omega_2^i, \ldots, \omega_n^i\}$ and $\Omega^j = \{\omega_1^j, \omega_2^j, \ldots, \omega_n^j\}$, the Bhattacharyya distance is as follows,

$$\mathcal{D}(\Omega^i, \Omega^j) = \sum_{k=1}^{n} \sqrt{\omega_k^i \omega_k^j}. \tag{6}$$

Hence, our mobility detector can identify a node is static or mobile based on an empirically measured threshold, $\mathcal{D}_T$.

IV. Implementation

In this section, we present the implementation issues. We implement CARA on the Impinj commercial reader using Low-Level Reader Protocol (LLRP) provided by EPCGlobal [11]. CARA is fully compliant with EPC Class-1 Gen-2 standard. Although different regions have different UHF regulations, our scheme generally applies to most regions [23].

Channel Probing

LLRP by default sets the channel dwell time to 2 seconds and the setting cannot be modified. Although 2 seconds are too long for channel probing (0.1 second is fairly enough), we have no choice but to comply with LLRP. Therefore, our prototype is actually a compromised implementation. In addition, we use the slowest rate to probe the channels, since high rate may cause channel errors, resulting in inaccurate channel quality estimation.

Channel Selection

In LLRP, we can predefine a hopping table which contains a list of channels to hop across. Once we are finished with channel selection, we configure the channel hopping table with the selected channels. The configuration incurs tens of milliseconds latency. Note that the maximum dwell time for a single channel is different across countries. For example, in North America, FCC allows up to 0.4 s for a single channel within 10 s. In Europe, it is only permitted to transmit on a single channel for 4 s if tags are being read and only 1 s if no tags are being read. In China, the maximum dwell time is 2 s.

Rate Selection

LLRP allows the reader to specify backward link data rate before starting inventory. Based on the EPC Class-1 Gen-2 standard, Impinj commercial reader provides us 5 kinds of backward link data rates, as listed in Table III. The data rate decreases from mode 0 to mode 1000. Changing the data rate requires restarting the inventory, which incurs tens of milliseconds latency.

Other than commercial readers, Buettner et al. developed a reader based on USRP software radio [24], which provides more flexibility in reader design. Nevertheless, the maximum output power of a USRP SBX daughterboard is 20dBm, which is far less than the Impinj commercial reader (maximum 32.5dBm), leading to a fairly short

TABLE III
BACKWARD LINK DATA RATES USED BY IMPINJ COMMERCIAL READER

Mode	Configuration
0	FM0 DR=8
1	M2 DR=8
2	M4 DR=8
3	M8 DR=8
1000	FM0 DR=64/3

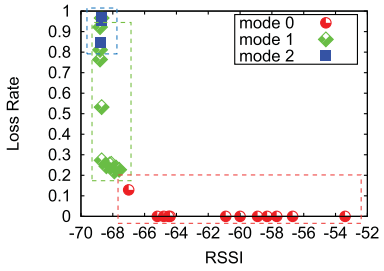

Fig. 11. Optimal rate mapping.

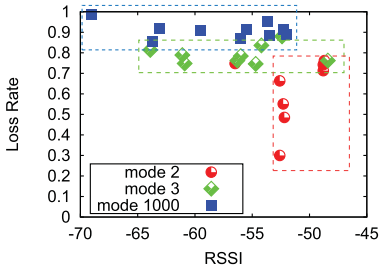

Fig. 12. Optimal rate mapping under interference.

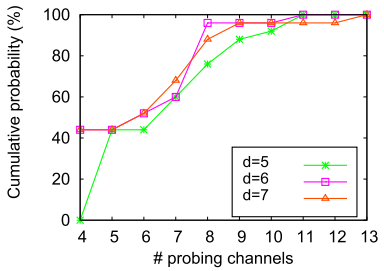

Fig. 13. CDF of the number of channels probed.

reading range. So the URSP reader is not a good option for our implementation.

V. EVALUATION

In this section, we evaluate our channel-aware rate adaptation framework CARA, through both experiments and trace-driven simulations. The experiments are conducted using Impinj Speedway reader and Impinj Inlay passive tags. We assume that the passive tags act as backscatter sensor nodes to transfer sensing data to the reader. This assumption is reasonable since backscatter nodes can split the buffered data into smaller pieces (with length 12 bytes) and take advantage of EPC message to transmit the data [25]. Here we just treat the tag EPC as sensing data. Moreover, we selectively put a URSP reader near the Impinj reader to cause external interference. The USRP reader transmits the same type of signal as the commercial reader, while its signal strength is weaker.

The evaluation consists of 5 parts. (1) Validating the chosen channel metrics. (2) Demonstrating the efficiency of selective channel probing. (3) Evaluating the accuracy of loss rate measurement (4) Benchmarking the effectiveness of channel selection algorithm. (5) Evaluating and comparing overall performance of CARA and BLINK under various environments.

A. Channel Metrics

We verify the effectiveness of two channel metrics, namely RSSI and packet loss rate. We place a tag in the reading range of a reader with different distances and orientations. Also, we conduct part of the experiments under interference emulated by a USRP reader. Then we examine the optimal data rate in each setting. In Figure 11 and Figure 12, the results show that packet loss rate is a more dominant feature than RSSI in choosing the optimal rate, since in most cases the optimal rate remains the same when RSSI varies. What is more, if there is no interference, the slowest rate chosen is mode 3, while the slowest rate chosen is mode 1000 under interference. This is reasonable since interference causes the undesirable channel quality. The different mapping results from 11 and 12 demonstrate that when interference is strong, the rate selection mapping should be recomputed, which is not considered in BLINK [9]. Therefore, BLINK may lead to wrong rate selection and reduce the throughput.

TABLE IV
AVERAGE PROBING ACCURACY

Probing interval	Probing accuracy
5	99.2%
6	96.9%
7	97.2%

B. Selective Channel Probing

In this section, we want to examine how to set the probing interval d?

First, we perform channel probing in 25 different environment settings with different probing intervals. In Figure 13, we depict the cumulative probability regarding the number of probed channels in selective probing. The probing accuracy results are also shown in Table IV. We find $d = 6$ is a good option because it has the highest CDF when the number of probed channel is 8, which is more than 90% probability. This means it can cut down the number of probed channels by half with the highest probability.

Also, we examine the impact of different d on the probing accuracy. The probing error rate is defined as the number of inaccurately measured channels divided by the total number of channels. Table IV summarizes the average probing error rate calculated from the 25 experiments with different probing intervals. We observe that no big differences exist among

TABLE V
MEASURED LOSS RATES USING ONE PROBE: MULTI-TAG VS 1-TAG

Number of tags	Loss rate (multi-tag)	Loss rate (1-tag)
1	0	0
2	0.4	0
3	0.5	0
4	0.7	0
5	0.95	0

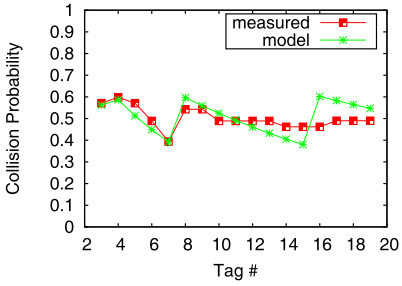

Fig. 14. Collision model.

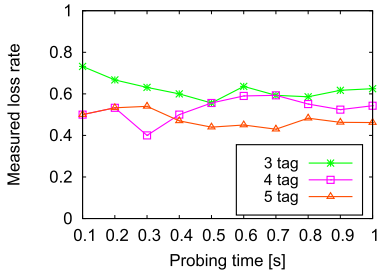

Fig. 15. Probing time.

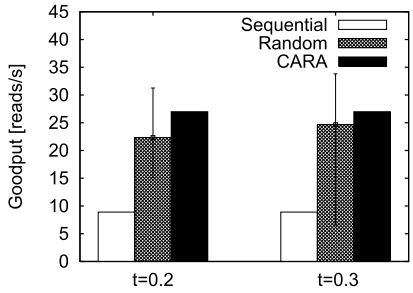

Fig. 16. Channel selection.

different choices among different d as they all achieve more than 95% accuracy. Combining the above two groups of results, we empirically set $d = 6$.

C. Packet Loss Rate

We evaluate the accuracy of loss rate measurement with respect to the number of tags and probing time.

Inaccuracy of One Probe Per Channel: BLINK proposes to use one probe to estimate channel quality without considering node collision. We first evaluate the effectiveness of this method in both one tag and multiple tags scenario. In one tag situation, we place a tag 10cm away from the reader antenna in a room without external interference. The reader reads the tag 20ms, which is approximately the time of 1 probe as claimed in [9]. Since the channel quality can be considered perfect, the expected loss rate is 0%. The experiment results coincide with our expectation. So we set the ground truth of packet loss rate to 0%.

Then we gradually increase the number of tags from 1 to 5 and conduct the same experiments. We present the measured packet loss rates in Table V. It can be seen that the measured loss rates from multiple tags deviate from those from a single tag (0%) as the number of tags increases. The reason behind is that tag collision happens when multiple tags contend for the channel to respond the probe. Therefore, it is clear that one probe will lead to inaccurate channel quality estimation in multiple tags scenario.

Collision Model Validation: Now we validate the accuracy of the proposed collision model. We put $3-19$ tags 10cm away from the reader antenna. In this situation, the expected path loss rate is 0%, so that the collision loss rate is equal to the packet loss rate which can be directly measured. We compare the measured collision loss rate with that calculated from our model. The results are shown in Figure 14. As the number of tags increases, the trend of our model basically follows the measured results. Therefore, our collision model is verified to be effective.

Choosing Appropriate Probing Time: Another question mentioned previously is how many probes are sufficient to obtain accurate packet loss rate, or equally how long should we probe each channel. We vary the probing time from 0.1s to 1s. In addition, we vary the number of tags to be 3, 4, and 5. The objective is to find the shortest time when the packet loss rate becomes stable, then this time should be chosen as optimal probing time. Figure 15 shows that the measured packet loss rate (without calibration) is relatively stable from 0.1s, so that we set 0.1s as the optimal probing time.

D. Channel Selection

In this section, we evaluate the effectiveness of our channel selection algorithm, using trace-driven simulation with a reader and 10 tags. To obtain the traces, we use the reader to sequentially scan all the channels and derive the RSSI and packet loss rate in each channel. Without loss of generality, we set the center frequency of USRP transmission signal to 920.63Hz, which overlaps with the frequency of channel 1 among the 16 channels. Note that in this case, not only the quality of channel 1 will be affected, but also several adjacent channels. Then the channel selection algorithm is run on top of the traces.

We compare our channel selection algorithm with two baseline schemes. The first one is to hop across all channels sequentially, denoted as sequential hopping. The second one is random channel hopping, in which the reader quickly switches to another channel when the packet loss rate for all tags are below a threshold t. We set t to 0.2 and 0.3. The comparison results are shown in Figure 16. Our channel selection approach outperforms both sequential hopping and random hopping, since it selects good channels that cover all the nodes. Sequential hopping suffers from poor channels and

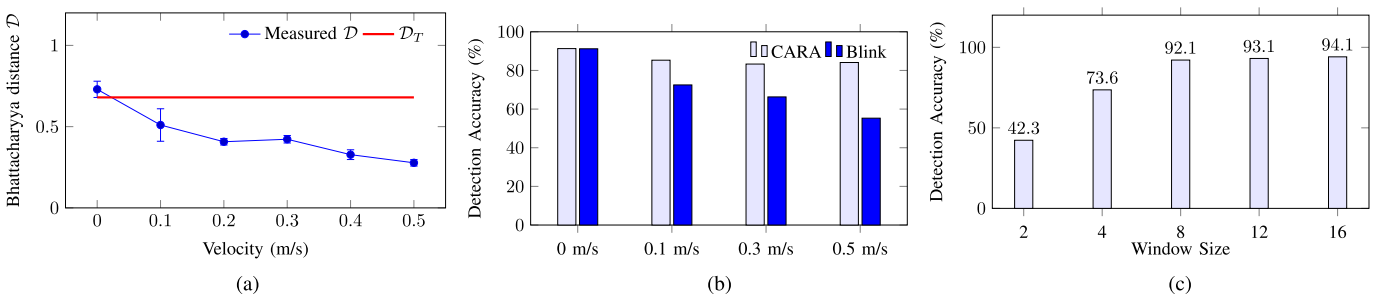

Fig. 17. Mobility evaluation for empirical thresholds and detection accuracy. (a) Empirical threshold for $\mathcal{D}_T$. (b) Detection accuracy comparison. (c) Impact of window size on detection accuracy

has the lowest efficiency. Random hopping can avoid poor channels to some extent but is quite unstable because of the randomness.

E. Mobility Detection

In this part, we evaluate our mobility detection module. First, we need to examine how to set the Bhattacharyya distance threshold, $\mathcal{D}_T$. In this test, we attach the tag on a programmable robot, iRobot Create 2, whose velocity can be controlled between 0-0.5 m/s by programming. The measured results of Bhattacharyya distance $\mathcal{D}_T$ are shown in Figure 17a. As expected, the Bhattacharyya distances under static and mobile scenarios are quite different. Specifically, when the tag is moving faster, $\mathcal{D}$ becomes smaller, which means the phase histograms tend to be less similar. Therefore, we use the minimum Bhattacharyya distance we measured in static scenarios as $\mathcal{D}_T$, which is 0.68. When the measured Bhattacharyya distance is more than 0.68, we mark the tag as static, otherwise mobile.

Next, we evaluate the mobility detection accuracy and compare it with BLINK. The results are included in Figure 17b. We have two observations from this test. First, when the tag is static, CARA achieves comparable detection accuracy as BLINK does. Second, when the tag is mobile, BLINK's accuracy degrades significantly while the accuracy of CARA, although degraded a bit, maintains above 80%. For example, BLINK only achieves 55.3% accuracy when the tag moves at 0.5 m/s. The main reason is that BLINK requires measured loss rates and RSSIs from all the channels to detect mobility. Under mobile scenarios, such a detection scheme does not have enough time to complete. For example, in North America, the typical settings are 50 channels and the 400 ms dwell time for each channel. So a full round of hopping takes 20 s. In China, the common settings are 16 channels and 2 s dwell time, which takes 32 s for hopping all the channels. In contrast, our scheme only requires a vector of phase readings. Intuitively, we want this vector to be long enough to get better accuracy. Through empirical results shown in Figure 17c, setting the window size at 8 is enough to get the detection accuracy above 90%.

Note that regarding computation overhead, the mobility detection schemes for both CARA and BLINK are lightweight. Specifically, the time complexity of CARA's mobility detection is $\mathcal{O}(w)$, where w is the window size of phase values

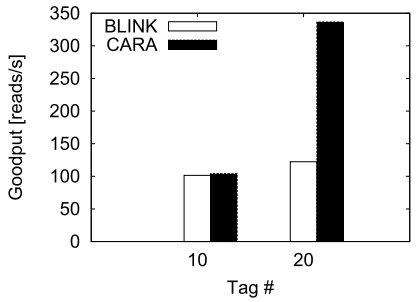

Fig. 18. Network goodput for 10 and 20 tags.

while that of BLINK is $\mathcal{O}(k)$, where k is the number of channels. Typically, $w = 8$ as aforementioned above and $k = 16$ if in China.

F. Overall Performance

We evaluate and compare the performance of CARA with the state-of-art work BLINK. Due to the limitation of Impinj readers, we use trace-driven simulation. The simulation is conducted with different number of tags, namely 10 and 20. What is more, to verify the efficiency of CARA in dynamic channel conditions, we also run the experiments under external interference emulated by a USRP reader. The interference strength is controlled by changing the transmitting power of USRP.

Figure 18 shows the overall network goodput without interference. When the tag population is 10, CARA and BLINK achieve similar goodputs. But when the tag population is 20, CARA achieves $2.75\times$ overall network goodput gain compared with BLINK. This performance gain comes from that CARA accurately estimate the loss rate and want to maximize the aggregate throughput while BLINK fails to consider. Note that as both CARA and BLINK can only choose a single rate for all the nodes, CARA cannot achieve better throughput for each node compared to BLINK. This is because no single rate can satisfy all the nodes in multi-rate wireless networks, e.g., WiFi [26], [27]. For 10 tags, we present the rate selection in Table VI and the corresponding per tag goodput in Figure 19. For some tags, such as tag 2, 4, 6, 7, 8, 9, 10, CARA chooses best rates while BLINK does not. Nevertheless, for tag 1, 3, and 5, BLINK outperforms CARA because CARA's choice is too aggressive, resulting in throughput loss. For tag 5,

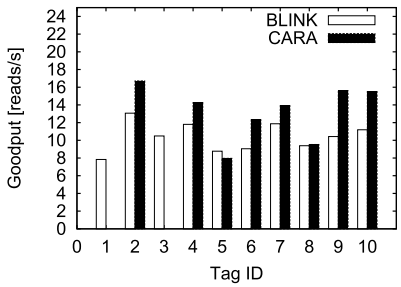

Fig. 19. Per tag goodput for 10 tags.

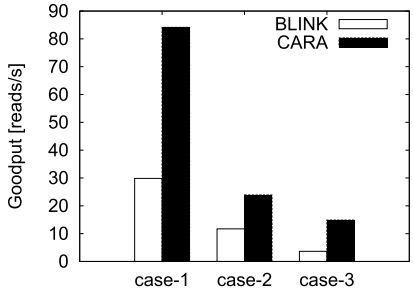

Fig. 20. The network goodput for 20 tags under interference.

even though the BLINK's choice is not optimal, its throughput is still a bit better than CARA, because its channel condition favors M8. Note that although BLINK tends to choose a lower rate because it may incorrectly count the MAC collisions into the loss rate, e.g., Table VI, it may also incorrectly select too aggressive rates sometime because its 1-probe strategy is too volatile. For example, the rate selection table of the 20-tag case is shown in Table VII. This time BLINK chooses an aggressive rate, M2, while CARA chooses M4. CARA benefits most of the tags. Therefore it achieves more than 2x aggregate throughput gain over BLINK. Note that even though for tag 9, 10, 17, 19, both rates of CARA and BLINK are not optimal, BLINK seems to outperform CARA. It is because throughput comparison results of two non-optimal rates are undetermined. This is also the reason why the rate of tag 8 for CARA is not optimal but still performs better than BLINK.

The overall network goodput under different interference strength is shown in Figure 20. The interference strength increases from case 1 to case 3. Some tags cannot be read by the reader if their goodput is 0. CARA outperforms BLINK under all three kinds of interference strength. In case 1, CARA is $2.8\times$ better than BLINK. Under case 2, the goodput of both schemes degrades because of stronger interference, while CARA still achieves $2\times$ goodput gain compared with BLINK. In case 3, CARA is $4.1\times$ better than BLINK. The reason why CARA exceeds under interference is that CARA's channel selection algorithm is able to avoid the interfered channels. In addition, we also provide the detailed per tag goodput under interference in Figure 21b-21d. Mostly, tags have better goodput in CARA than in BLINK.

Furthermore, we investigate the performance of our burstiness-aware scheme by comparing CARA to Blink and CARA- that is CARA without quantifying burstiness.

TABLE VI
RATE SELECTION FOR 10 TAGS IN FIGURE 19

Tag	Optimal Rate	Rate of CARA	Rate of BLINK
1	M8 DR=8	M2 DR=8	M8 DR=8
2	M2 DR=8	M2 DR=8	M8 DR=8
3	M8 DR=8	M2 DR=8	M8 DR=8
4	M2 DR=8	M2 DR=8	M8 DR=8
5	M4 DR=8	M2 DR=8	M8 DR=8
6	M2 DR=8	M2 DR=8	M8 DR=8
7	M2 DR=8	M2 DR=8	M8 DR=8
8	M2 DR=8	M2 DR=8	M8 DR=8
9	M2 DR=8	M2 DR=8	M8 DR=8
10	M2 DR=8	M2 DR=8	M8 DR=8

TABLE VII
RATE SELECTION FOR 20 TAGS IN FIGURE 21a

Tag	Optimal Rate	Rate of CARA	Rate of BLINK
1	M4 DR=8	M4 DR=8	M2 DR=8
2	M4 DR=8	M4 DR=8	M2 DR=8
3	M4 DR=8	M4 DR=8	M2 DR=8
4	M4 DR=8	M4 DR=8	M2 DR=8
5	M4 DR=8	M4 DR=8	M2 DR=8
6	M4 DR=8	M4 DR=8	M2 DR=8
7	M4 DR=8	M4 DR=8	M2 DR=8
8	M8 DR=8	M4 DR=8	M2 DR=8
9	M8 DR=8	M4 DR=8	M2 DR=8
10	M8 DR=8	M4 DR=8	M2 DR=8
11	M4 DR=8	M4 DR=8	M2 DR=8
12	M4 DR=8	M4 DR=8	M2 DR=8
13	M4 DR=8	M4 DR=8	M2 DR=8
14	M4 DR=8	M4 DR=8	M2 DR=8
15	M4 DR=8	M4 DR=8	M2 DR=8
16	M4 DR=8	M4 DR=8	M2 DR=8
17	M8 DR=8	M4 DR=8	M2 DR=8
18	M4 DR=8	M4 DR=8	M2 DR=8
19	M8 DR=8	M4 DR=8	M2 DR=8
20	M4 DR=8	M4 DR=8	M2 DR=8

We conduct comparisons under different levels of burstiness, high, intermediate, and low burstiness. As shown in Figure 22d, CARA consistently outperforms CARA- and Blink in all levels of burstiness, especially in the high burstiness case. Specifically, the goodput of CARA is $1.73\times$ and $1.94\times$ better than CARA- and Blink when burstiness is high. Such performance gain should be attributed to our burstiness-aware scheme that chooses consistently good links and avoids consistently bad links. Similar observations can be made when the number of tags increases to 15 and 20, shown in Figure 22e-22f.

VI. RELATED WORK

Frequency and Spatial Diversity in Backscatter Networks

The frequency diversity in backscatter communication networks has been studied in [28]–[33]. Similar to our work, they

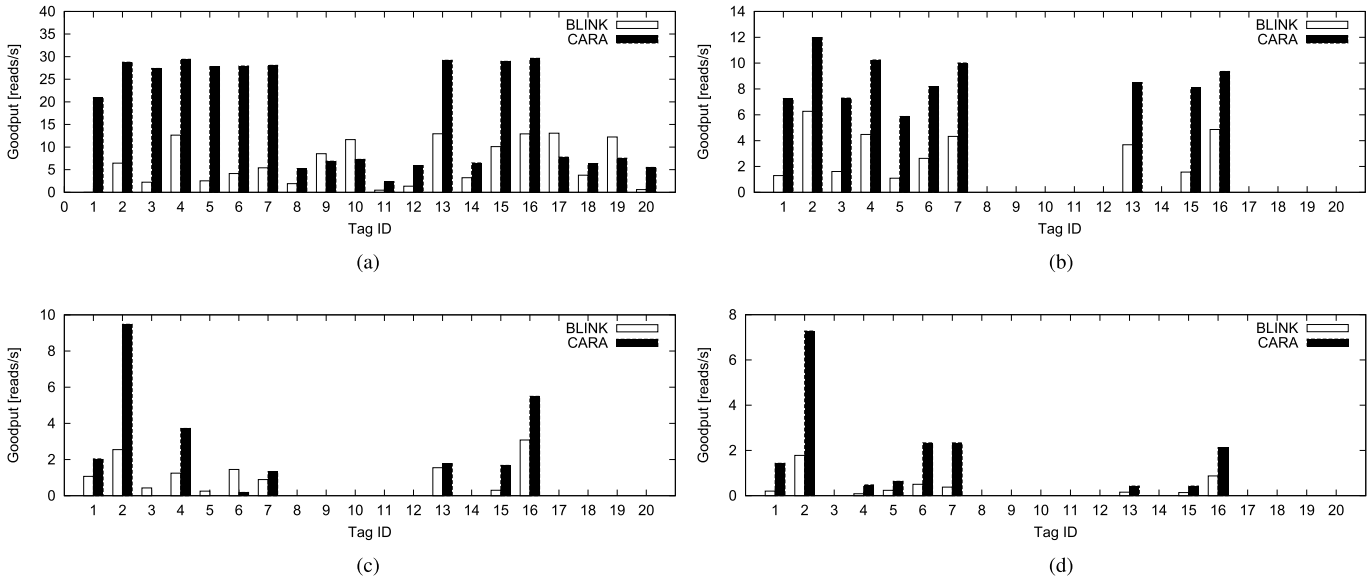

Fig. 21. Per tag goodput under different interference strengths. (a) Per tag goodput for 20 tags. (b) Per tag goodput for 20 tags under interference: case 1. (c) Per tag goodput for 20 tags under interference: case 2. (d) Per tag goodput for 20 tags under interference: case 3.

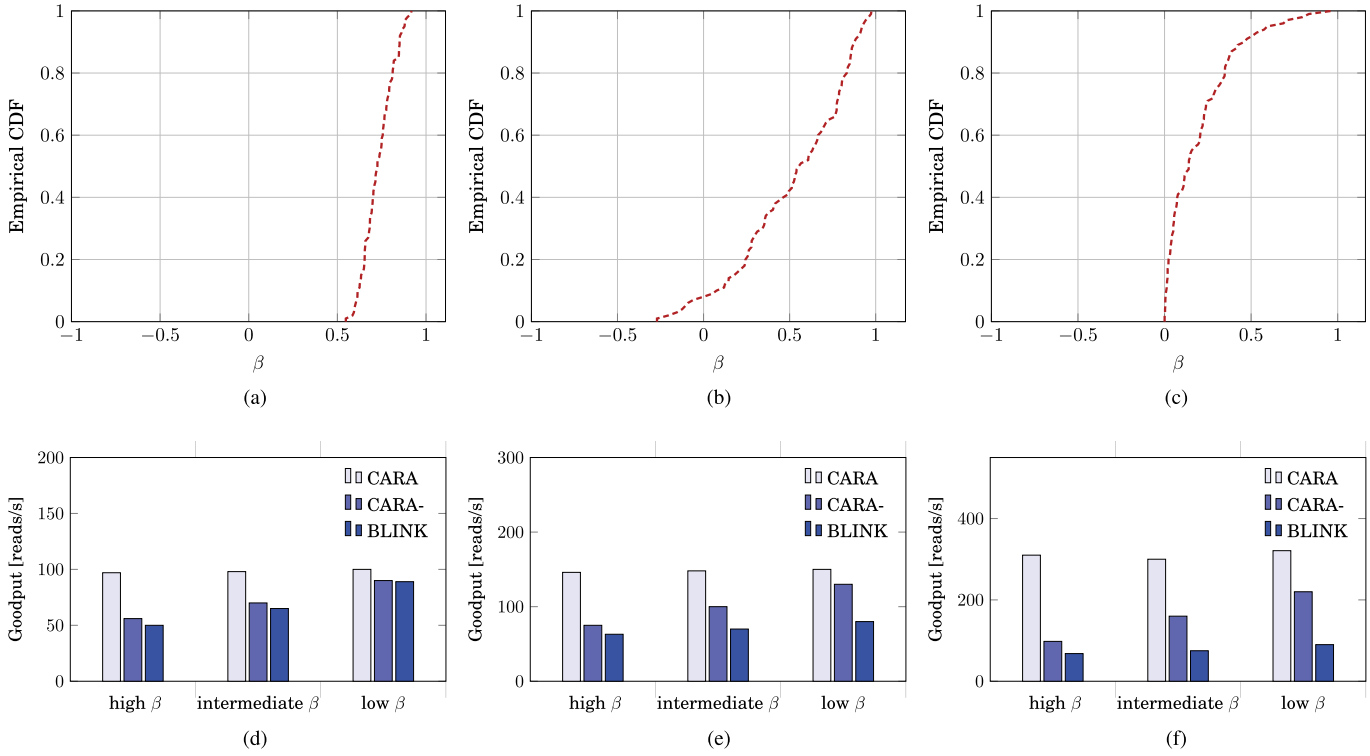

Fig. 22. Comparisons of CARA, CARA-, and Blink under different levels of burstiness. Three representative empirical CDFs are shown in (a)–(c). Comparisons are done with different numbers of tags shown in (d)–(f). We can see that only CARA can maintain high performance under different levels of burstiness while the goodputs of CARA- and Blink degrade significantly with bursty links.

claim that multipath effect impacts UHF signal propagation, particularly in indoor environments. The spatial diversity is also discovered and discussed in [34]. Our work is motivated by these findings. The difference is that we exploit these characteristics to enable more accurate rate adaptation.

Rate Adaptation

The impact of data rate on packet loss and bit error rate (BER) is studied in 802.11 and cellular networks [26] [35]. Based on the studies, various rate adaptation schemes [36]–[41] are proposed in recent years primarily in 802.11 networks. The key idea is to estimate the channel quality with channel metrics and adapt the data rate accordingly. The widely adopted metrics include link layer metrics such as packet loss [39], and PHY metrics such as SNR [39], [40] and BER [41]. The applicability of previous work to our problem is limited since the communication modes are fundamentally different. Unlike active radios, the low power feature

of backscatter communication makes it more vulnerable to channel dynamics, especially multipath effect. In addition, the forward links and backward links in backscatter communication are highly asymmetric, resulting in different modulation and coding schemes. Existing rate adaptation approaches in backscatter communication networks include BLINK [9] and Buzz [10]. Different from these two designs, our scheme is aware of channel diversity, including spatial and frequency diversity. Nevertheless, in [9] and [10], one of them is ignored.

Channel Selection

Channel selection is studied in [42] and [43] in 802.15.4 multi-channel networks. These approaches propose to take advantage of the channel diversity in multi-channel scenarios. Our work is similar to them in this sense, except that we focus on rate adaptation and channel selection is only one component of the framework.

PHY and MAC Optimization

There are also many works focusing on throughput optimization in the PHY and MAC layers. Flit [25] enables transferring bulk data in a burst and thus largely reduces collisions on the MAC layer. On the PHY layer, Laissez-Faire [44] and BiGroup [45] propose to decode parallel up-link transmissions by separating signals in both the time and IQ domains. Nevertheless, those works are not fully compliant with the C1G2 protocol and commercial readers.

VII. Conclusion

This paper has proposed a channel-aware rate adaptation framework that exploits channel diversity, including spatial and frequency diversity. A lightweight channel probing scheme and a novel channel selection algorithm have been presented to enable throughput gain. We have also described a mobility detection method using difference of phase profiles to further save probing overhead. Extensive experiments have been done to demonstrate a large throughput improvement compared with state-of-the-art approaches.

References

[1] M. Buettner, B. Greenstein, A. Sample, J. R. Smith, and A. Wetherall, "Revisiting smart dust with RFID sensor networks," in *Proc. HotNets-VII*, 2008, pp. 1–132.

[2] D. J. Yeager, P. S. Powledge, R. Prasad, D. Wetherall, and J. R. Smith, "Wirelessly-charged UHF tags for sensor data collection," in *Proc. IEEE RFID*, Apr. 2008, pp. 320–327.

[3] J. R. Smith, A. P. Sample, P. S. Powledge, S. Roy, and A. Mamishev, "A wirelessly-powered platform for sensing and computation," in *Proc. Ubicomp*, 2006, pp. 495–506.

[4] R. Want, "Enabling ubiquitous sensing with RFID," *Computer*, vol. 37, no. 4, pp. 84–86, 2004.

[5] A. Wang, V. Iyer, V. Talla, J. R. Smith, and S. Gollakota, "FM backscatter: Enabling connected cities and smart fabrics," in *Proc. USENIX NSDI*, 2017, pp. 1–16.

[6] S. Caizzone and G. Marrocco, "RFID-grids for deformation sensing," in *Proc. IEEE Antennas Propag. Soc. Int. Symp. (APSURSI)*, Apr. 2012, pp. 130–134.

[7] J. S. Besnoff and M. S. Reynolds, "Near field modulated backscatter for *in vivo* biotelemetry," in *Proc. IEEE RFID*, Apr. 2012, pp. 135–140.

[8] D. Tse and P. Viswanath, *Fundamentals of Wireless Communication*. Cambridge, U.K.: Cambridge Univ. Press, 2005.

[9] P. Zhang, J. Gummeson, and D. Ganesan, "BLINK: A high throughput link layer for backscatter communication," in *Proc. ACM MobiSys*, 2012, pp. 92–112.

[10] J. Wang, H. Hassanieh, D. Katabi, and P. Indyk, "Efficient and reliable low-power backscatter networks," in *Proc. ACM SIGCOMM*, 2012, pp. 61–72.

[11] (2007). *EPC Radio-Frequency Identity Protocols Class-1 Generation-2 UHF RFID Protocol for Communications at 860 MHz–960 MHz*. [Online]. Available: http://www.gs1.org/gsmp/kc/epcglobal/uhfc1g2/uhfc1g2_1_1_0-standard-20071017.pdf

[12] V. V. Vazirani, *Approximation Algorithms*. Berlin, Germany: Springer-Verlag, 2004.

[13] K. Srinivasan, M. A. Kazandjieva, S. Agarwal, and P. Levis, "The β-factor: Measuring wireless link burstiness," in *Proc. ACM SenSys*, 2008, pp. 1–14.

[14] Y. Rubner, C. Tomasi, and L. J. Guibas, "A metric for distributions with applications to image databases," in *Proc. IEEE ICCV*, Jan. 1998, pp. 59–66.

[15] N. Golmie, N. Chevrollier, and O. Rebala, "Bluetooth and WLAN coexistence: Challenges and solutions," *IEEE Wireless Commun.*, vol. 10, no. 6, pp. 22–29, Dec. 2003.

[16] S.-H. Lee and Y.-H. Lee, "Adaptive frequency hopping for Bluetooth robust to WLAN interference," *IEEE Commun. Lett.*, vol. 13, no. 9, pp. 628–630, Sep. 2009.

[17] W. Bronzi, R. Frank, G. Castignani, and T. Engel, "Bluetooth low energy performance and robustness analysis for inter-vehicular communications," *Ad Hoc Netw.*, vol. 37, pp. 76–86, Feb. 2016.

[18] L. Yang *et al.*, "Tagoram: Real-time tracking of mobile RFID tags to high precision using COTS devices," in *Proc. ACM MobiCom*, 2014, pp. 1–12.

[19] W. Gong, S. Chen, J. Liu, and Z. Wang, "MobiRate: Mobility-aware rate adaptation using PHY information for backscatter networks," in *Proc. IEEE INFOCOM*, Honolulu, HI, USA, Apr. 2018.

[20] *Low Level Reader Protocol Standard*. Accessed: Feb. 17, 2018. [Online]. Available: http://www.gs1.org/gsmp/kc/epcglobal/llrp

[21] L. Shangguan and K. Jamieson, "The design and implementation of a mobile RFID tag sorting robot," in *Proc. ACM MobiSys*, 2016, pp. 31–42.

[22] A. Bhattacharyya, "On a measure of divergence between two statistical populations defined by their probability distributions," *Bull. Calcutta Math. Soc.*, vol. 35, pp. 99–109, 1943.

[23] *UHF Regulations*. Accessed: Feb. 17, 2018. [Online]. Available: http://www.gs1.org/docs/epc/UHF_Regulations.pdf

[24] *Universal Software Radio Peripheral*. Accessed: Feb. 17, 2018. [Online]. Available: http://www.ettus.com/

[25] J. Gummeson, P. Zhang, and D. Ganesan, "Flit: A bulk transmission protocol for RFID-scale sensors," in *Proc. ACM MobiSys*, 2012, pp. 71–84.

[26] D. Aguayo, J. Bicket, S. Biswas, G. Judd, and R. Morris, "Link-level measurements from an 802.11b mesh network," in *Proc. ACM SIGCOMM*, 2004, pp. 1–11.

[27] L. Sun, S. Sen, and D. Koutsonikolas, "Bringing mobility-awareness to WLANs using PHY layer information," in *Proc. ACM CoNEXT*, 2014, pp. 53–66.

[28] W.-C. Lai, J.-F. Huang, C.-M. Hsu, and P.-G. Yang, "Low power VCO and mixer for computing miracast and mobile Bluetooth applications," in *Proc. IEEE Cyberc*, Oct. 2014, pp. 425–428.

[29] D. Qiao and K. G. Shin, "Achieving efficient channel utilization and weighted fairness for data communications in IEEE 802.11 WLAN under the DCF," in *Proc. IEEE IWQoS*, May 2002, pp. 227–236.

[30] *IEEE Standard for Information technology– Local and metropolitan area networks—Specific requirements—Part 11: Wireless LAN Medium Access Control (MAC)and Physical Layer (PHY) Specifications Amendment 5: Enhancements for Higher Throughput*, IEEE Standard ANSI/IEEE 802.11n-2009, 2009. [Online]. Available: http://standards.ieee.org/getieee802/download/802.11n-2009.pdf

[31] H. Rahul, F. Edalat, D. Katabi, and C. G. Sodini, "Frequency-aware rate adaptation and MAC protocols," in *Proc. ACM MobiCom*, 2009, pp. 193–204.

[32] A. Lázaro, D. Girbau, and D. Salinas, "Radio link budgets for UHF RFID on multipath environments," *IEEE Trans. Antennas Propag.*, vol. 57, no. 4, pp. 1241–1251, Apr. 2009.

[33] M. Buettner and D. Wetherall, "An empirical study of UHF RFID performance," in *Proc. ACM Mobicom*, 2008, pp. 223–234.

[34] S. R. Banerjee, R. Jesme, and R. A Sainati, "Investigation of spatial and frequency diversity for long range UHF RFID," in *Proc. IEEE Antennas Propag. Soc. Int. Symp.*, Jul. 2008, pp. 1–4.

[35] K. Balachandran, S. R. Kadaba, and S. Nanda, "Channel quality estimation and rate adaptation for cellular mobile radio," *IEEE J. Sel. Areas Commun.*, vol. 17, no. 7, pp. 1244–1256, Jul. 1999.

[36] G. Holland, N. Vaidya, and P. Bahl, "A rate-adaptive MAC protocol for multi-hop wireless networks," in *Proc. ACM MobiCom*, 2001, pp. 236–251.
[37] B. Sadeghi, V. Kanodia, A. Sabharwal, and E. Knightly, "Opportunistic media access for multirate ad hoc networks," in *Proc. ACM MobiCom*, 2002, pp. 24–35.
[38] M. Lacage, M. H. Manshaei, and T. Turletti, "IEEE 802.11 rate adaptation: A practical approach," in *Proc. ACM MSWiM*, Oct. 2004, pp. 126–134.
[39] S. H. Wong, H. Yang, S. Lu, and V. Bharghavan, "Robust rate adaptation for 802.11 wireless networks," in *Proc. ACM MobiCom*, 2006, pp. 146–157.
[40] J. Camp and E. Knightly, "Modulation rate adaptation in urban and vehicular environments: Cross-layer implementation and experimental evaluation," in *Proc. ACM MobiCom*, 2008, pp. 1949–1962.
[41] M. Vutukuru, H. Balakrishnan, and K. Jamieson, "Cross-layer wireless bit rate adaptation," in *Proc. ACM SIGCOMM*, 2009, pp. 1–12.
[42] M. Doddavenkatappa, M.-C. Chan, and B. Leong, "Improving link quality by exploiting channel diversity in wireless sensor networks," in *Proc. IEEE RTSS*, Nov./Dec. 2011, pp. 159–169.
[43] H. K. Le, D. Henriksson, and T. Abdelzaher, "A practical multi-channel media access control protocol for wireless sensor networks," in *Proc. ACM IPSN*, 2008, pp. 70–81.
[44] P. Hu, P. Zhang, and D. Ganesan, "Laissez-faire: Fully asymmetric backscatter communication," in *Proc. ACM SIGCOMM*, 2015, pp. 255–267.
[45] J. Ou, M. Li, and Y. Zheng, "Come and be served: Parallel decoding for COTS RFID tags," *IEEE/ACM Trans. Netw.*, vol. 25, no. 3, pp. 1569–1581, Jun. 2017.

Wei Gong (M'14) received B.S. degree from the Department of Computer Science and Technology, Huazhong University of Science and Technology, the M.S. degree from the School of Software, Tsinghua University, and Ph.D. degree from the Department of Computer Science and Technology, Tsinghua University. His research interests include backscatter communication, distributed computing, and the Internet-of-Things applications.

Haoxiang Liu received the B.S. degree from the Department of Computer Science and Technology, Shanghai Jiao Tong University, Shanghai, China, in 2007, and the Ph.D. degree from the Department of Computer Science and Engineering, The Hong Kong University of Science and Technology. His research interests include RFID applications and mobile computing.

Jiangchuan Liu (S'01–M'03–SM'08–F'17) received the B.Eng. degree (*cum laude*) in computer science from Tsinghua University, Beijing, China, in 1999, and the Ph.D. degree in computer science from The Hong Kong University of Science and Technology in 2003. He is currently a University Professor with the School of Computing Science, Simon Fraser University, BC, Canada. He is an NSERC E.W.R. Steacie Memorial Fellow. He is a Steering Committee Member of the IEEE TRANSACTIONS ON MOBILE COMPUTING. He was a co-recipient of the inaugural Test of Time Paper Award of IEEE INFOCOM in 2015, the ACM SIGMM TOMCCAP Nicolas D. Georganas Best Paper Award in 2013, and the ACM Multimedia Best Paper Award in 2012. He has served on the Editorial Boards for the IEEE/ACM TRANSACTIONS ON NETWORKING, the IEEE TRANSACTIONS ON BIG DATA, the IEEE TRANSACTIONS ON MULTIMEDIA, the IEEE COMMUNICATIONS SURVEYS AND TUTORIALS, and the IEEE INTERNET OF THINGS JOURNAL.

Xiaoyi Fan (S'14) received the B.E. degree from the Beijing University of Posts and Telecommunications, Beijing, China, in 2013, and the M.Sc. degree from Simon Fraser University, BC, Canada, in 2015. He is currently pursuing the Ph.D. degree with the School of Computing Science, Simon Fraser University. His areas of interest are cloud computing, big data, and mobile computing.

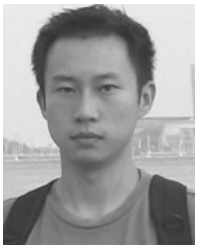

Kebin Liu (M'08) received the B.S. degree from the Department of Computer Science, Tongji University, the M.S. degree from Shanghai Jiao Tong University, China, and the Ph.D. degree from the Department of Computer Science and Engineering, Shanghai Jiao Tong University. He is currently an Assistant Researcher with Tsinghua University. His current research interests include sensor networks and distributed systems.

Qiang Ma (S'11–M'14) received the B.S. degree from the Department of Computer Science and Technology, Tsinghua University, China, in 2009, and the Ph.D. degree from the Department of Computer Science and Engineering, The Hong Kong University of Science and Technology, in 2013. He is currently an Assistant Researcher with Tsinghua University. His research interests include sensor networks and mobile computing.

Xiaoyu Ji (S'13–M'15) received the bachelor's degree in electronic information technology from Zhejiang University, Hangzhou, China, in 2010, and the Ph.D. degree from the Department of Computer Science, The Hong Kong University of Science and Technology, in 2015. He joined the Department of Electrical Engineering, Zhejiang University, in 2016, as an Assistant Professor.